Statistical Modeling of the 1997-1998 Colfiorito Earthquake Sequence

THE SEISMOLOGICAL SOCIETY OF AMERICA
400 Evelyn Ave., Suite 201
Albany, CA 94706-1375
(510) 525-5474; FAX (510) 525-7204
www.seismosoc.org

Bulletin of the Seismological Society of America, Vol. 104, No. 2, pp. 885–897, April 2014, doi: 10.1785/0120130270

Statistical Modeling of the 1997–1998 Colfiorito Earthquake Sequence: Locating a Stationary Solution within Parameter Uncertainty

by Sarah Touati, Mark Naylor, and Ian G. Main

Abstract The Umbria–Marche region of Italy is a seismically active region that experienced a strong sequence of earthquakes during 1997–1998, with a cluster of magnitude $M \geq 5$ events, during which the average event rate increased from the long-term level by several orders of magnitude. Using maximum-likelihood (ML) inversion of the epidemic-type aftershock sequences model to characterize the seismicity of this region over 22 years, we find, in agreement with previous studies, the event rate during the sequence is underpredicted, based on simulations with the large $M \geq 5$ events fixed. However, by sampling the parameter space around the ML solution within the inversion uncertainty and comparing the simulated event rate with that of the real data, we are able to find near-maximum-likelihood parameters that provide a reasonable match to both the long-term average event rate and the rate during the sequence. We use the shape of the interevent time histogram to infer that the events in the sequence are probably mostly aftershocks of the large events, rather than an increased occurrence of background events. We suggest that event rate comparisons can be useful as an additional constraint on the selection of parameters from within the 95% confidence interval of the ML fit. Our results demonstrate the extra constraint can greatly improve the match between a stationary model and finite catalog data and that care is needed before adding further parameters to ascribe nonstationarity to time-dependent event rate changes.

Introduction

The Umbria–Marche region of Italy is a seismically active area that experienced a particularly strong sequence of earthquakes during 1997–1998, during which the event rate peaked to several orders of magnitude higher than the long-term average. Following the work of Lombardi *et al.* (2010), our questions concern the nature of this sequence and to what extent it needs to be considered as a statistical deviation from the usual seismicity pattern of the region or, instead, whether it may be viewed as a chance fluctuation that is still consistent with the long-term activity. Essentially, we seek to determine whether the seismicity of this period is consistent with a stationary long-term activity, produced mostly by tectonic loading, or is nonstationary, for example due to episodic fluid movement (CO_2 degassing from limestone, or volcanic activity; e.g., Miller *et al.*, 2004; Traversa and Grasso, 2010).

Like Lombardi *et al.* (2010), we use the epidemic-type aftershock sequences (ETAS) model in our analysis (Ogata, 1988, 1998). ETAS is a benchmark statistical model for earthquake occurrence and, as such, is widely used to represent regional tectonic seismicity through maximum-likelihood (ML) estimated parameter values (Zhuang *et al.*, 2012). It accounts for several known sources of rate fluctuations: a basic Poisson process of independent events, representing the effect of stationary tectonic loading; potential aftershock triggering from every event in the catalog (including aftershocks of other events), with a time-decaying rate defined by the Omori law, and at an absolute rate that increases exponentially with the magnitude of the triggering event; and independent selection of the magnitudes of all events from, usually, the Gutenberg–Richter distribution. A variant of the model, including spatial coordinates of events, additionally takes into account the aftershock clustering in space, with a variety of empirical distribution functions in use. The ETAS model is thus capable of accounting for event rates that fluctuate in time and space according to its conditional intensity function:

$$\lambda(t|H_t) = \mu + A\sum_{i:t<t_i} \exp[\alpha(M_i - M_0)]\left(1 + \frac{t - t_i}{c}\right)^{-p} \quad (1)$$

or, for a spatial ETAS model using Zhuang *et al.*'s spatial aftershock distribution (Zhuang *et al.*, 2002; Harte, 2012),

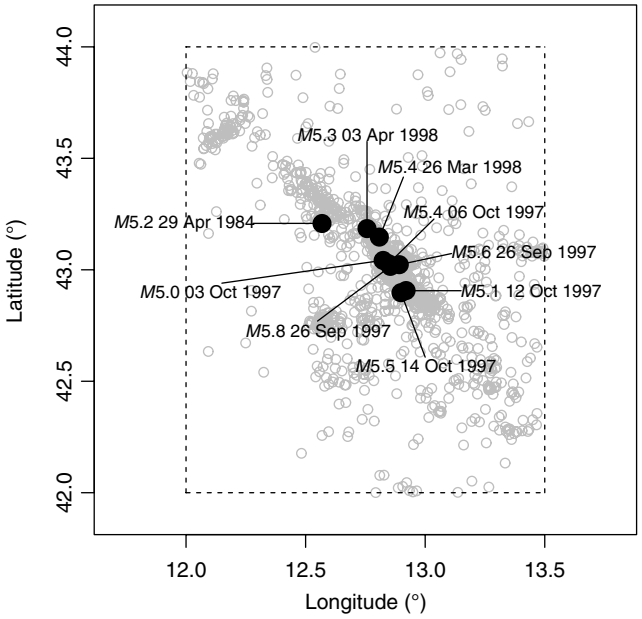

Figure 1. The locations of the Colfiorito dataset events (open circles), with large filled circles indicating the $M \geq 5$ events. A dashed line shows the geographical boundaries of the dataset.

$$\lambda(t,x,y|H_t) = \mu' + A\sum_{i:t<t_i} \exp[\alpha(M_i - M_i)]\left(1 + \frac{t-t_i}{c}\right)^{-p} \times \frac{1}{2\pi d \exp[\alpha(M_i - M_i)]} \times \exp\left(-\frac{1}{2}\frac{x^2+y^2}{d\exp[\alpha(M_i - M_i)]}\right), \quad (2)$$

in which t_i are the times of the past events and M_i are their magnitudes; μ is the independent or background event rate; A, c, and p are parameters of the Omori law; and α is the productivity parameter. The spatial aftershock distribution thus described is a 2D Gaussian with variance $\sigma^2 = de^{\alpha(M_i - M_0)}$, giving d as a further parameter for the spatial ETAS model. (Note that μ' in the spatial model is the background rate per unit area as well as per unit time, so integration of the model over all space recovers the temporal-only model.)

Lombardi *et al.* (2010) try to fit the stationary ETAS model to earthquakes in the Colfiorito region, both for the full catalog duration of 22 years and for a 15-month period containing the sequence, and use statistical tests and analytic prediction to assess the goodness of fit. They find that in both cases the optimal ML solution does not adequately account for the event rate rise during the sequence. They then include a background rate that varies in time with a moving window of 10 days during the sequence and find a significantly improved fit to the data that is approved by statistical tests. They interpret this result in terms of a fluid signal from within the crust: fluid signals usually show up as swarms and are modeled as an elevated background rate.

In this paper, we use a forward-modeling (simulation) approach to retest the null hypothesis that the sequence is mostly aftershocks that follow the same statistical pattern as that inferred for the rest of the data but which are especially prolific here due to the presence of several large events (which may be a chance outcome of a single realization). We begin by examining the data, inverting ML ETAS parameters on a variety of subsets of the data, and simulating the catalog with the largest events added in to compare the event rate throughout. We then explore whether the fit can be improved by sampling around the ML solution within the uncertainty. Finally, we consider whether the large events that we have transplanted from the catalog are likely to have arisen in our model or require additional explanation.

Table 1
Details of the Largest Events ($M \geq 5$) in the Colfiorito Dataset

Date (yyyy/mm/dd)	Time (hh:mm:ss)	Latitude (°)	Longitude (°)	Magnitude
1984/04/29	05:03:00	43.21	12.57	5.2
1997/09/26	00:33:13	43.02	12.89	5.6
1997/09/26	09:40:27	43.01	12.85	5.8
1997/10/03	08:55:22	43.04	12.82	5.0
1997/10/06	23:24:53	43.03	12.85	5.4
1997/10/12	11:08:37	42.91	12.92	5.1
1997/10/14	15:23:11	42.90	12.90	5.5
1998/03/26	16:26:17	43.15	12.81	5.4
1998/04/03	07:26:37	43.19	12.76	5.3

Properties of the Colfiorito Data

We consider the same data analyzed in Lombardi *et al.* (2010), a subset of the Catalogo della Sismicità Italiana—CSI 1.1 (Castello *et al.*, 2005, 2007) comprising events occurring in the Umbria–Marche region. The data are 1527 events of $M \geq 2.5$, derived from the timespan of the CSI (the years 1981–2002, inclusive) and occurring between 12° and 13.5° longitude and 42° and 44° latitude. We will call this the Colfiorito dataset. Lombardi *et al.* (2010) analyzed the completeness threshold for this data; they found that it varies with time but is not higher than M 2.5 at any point in this period. The Bollettino Sismico Italiano catalog takes over the recording of Italian earthquakes from 2002 onward, but, because the period 2002–2005 is unofficial and only consistent with CSI data above magnitude 3.5 (Romashkova and Peresan, 2013), we do not use it.

The data contain nine events of magnitude $M \geq 5$: the first occurs on 29 April 1984, and the rest occur in two clusters, with six events recorded within 19 days between 26 September 1997 and 14 October 1997 and a further two on 26 March and 3 April 1998. Figure 1 highlights these events on a map of the Colfiorito dataset, and Table 1 lists the event details. The sequence period defined in Lombardi *et al.* (2010) runs for a 15-month period from 3 May 1997 to 17 August 1998, encompassing both of these clusters. Figure 2a shows the month-by-month mean event rate for the Colfiorito dataset (1981–2002), along with the positions

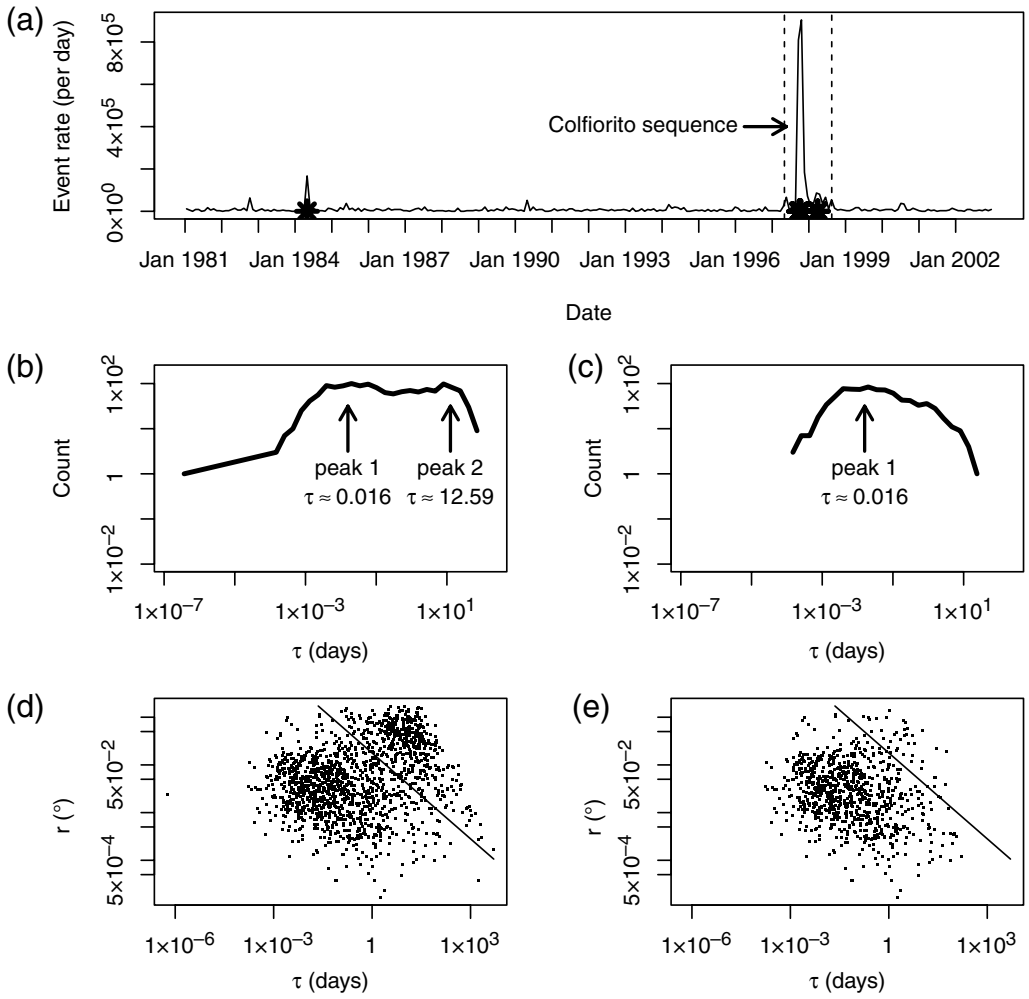

Figure 2. The Colfiorito dataset: (a) month-by-month mean event rate, with stars indicating the occurrence times of the large $M \geq 5$ events; interevent time histogram for (b) the whole dataset and (c) the sequence period only (3 May 1997–17 August 1998); space–time nearest-neighbor for each event in (d) the whole dataset and (e) the sequence period only (3 May 1997–17 August 1998). In (d) and (e), the straight line represents an approximate divide between the two clusters observed in (d), described more fully in the text.

of the $M \geq 5$ events; the sequence of 1997–1998 is clearly visible as a large temporary peak in the event rate.

The distribution of interevent times, in both the ETAS model and in real tectonic earthquakes, is generally bimodal (Lindman *et al.*, 2005; Touati *et al.*, 2009, 2011), a superposition of a gamma distribution component arising from aftershock sequences and an exponential component that results from the consecutive occurrence of unrelated events (i.e., either independent background or aftershocks belonging to separate sequences) (Touati *et al.*, 2009). When aftershock sequences moderately overlap in time, as for a regional-scale catalog, this bimodality can result in an overall distribution that resembles a gamma distribution (Molchan, 2005; Saichev and Sornette, 2006, 2007; Touati *et al.*, 2009), as the crossover between the two peaks forms an approximate power-law segment (a straight line in a log–log plot). Figure 2b and 2c shows the interevent intervals for the whole Colfiorito dataset and the 15-month sequence period, respectively, in logarithmic histograms. (Unlike probability density estimates, the counts are not normalized by either bin width or total count; we prefer simple histograms for clearly showing the structure of the data.) The whole-data histogram is consistent with a regional case, showing the typical broadband plateau between the two components, which, if they could be plotted separately, would be expected to have peaks in this plot at roughly the positions of the two arrows: at the start of the plateau for the aftershocks component, and just before the exponential decay for the independent events component. In contrast, the histogram for the sequence period is single peaked, with a peak that coincides with the short-term (aftershock) component of the whole-data plot, and exhibits a possible power-law decay toward longer interevent times, as expected for an aftershock sequence. This is an early indication that the sequence may consist mostly of aftershocks with little background or temporal overlapping to interrupt the Omori signature.

Finally, in Figure 2d and 2e, a point is plotted for each event, indicating its nearest neighbor based on a combined

Table 2
Results of ETAS Inversions on the Colfiorito Data

Inversion Case	μ (Per Day)	A	α	c (Days)	p	n
Colfiorito dataset (1981–2002)	0.043 ± 0.003	1.455 ± 0.302	1.679 ± 0.068	0.037 ± 0.008	1.230 ± 0.028	0.824
Sequence (15 months)	0.117 ± 0.032	2.538 ± 0.694	1.418 ± 0.096	0.042 ± 0.012	1.317 ± 0.050	0.861
Subsequence (6 months)	0.087 ± 0.055	0.913 ± 0.378	1.819 ± 0.129	0.074 ± 0.023	1.336 ± 0.060	0.894

Table 3
Comparison of Real and Simulated Average Event Rate (Per Day)

Case	Whole Dataset Event Rate (1981–2002), Per Day	Sequence Event Rate (15 Months), Per Day	Subsequence Event Rate (6 Months), Per Day
Colfiorito data	0.190	1.828	3.861
ETAS fitted to Colfiorito dataset (1981–2002)	0.197 ± 0.018	1.288 ± 0.162	2.420 ± 0.347
ETAS fitted to sequence (15 months)	0.572 ± 0.041	1.754 ± 0.248	2.968 ± 0.520
ETAS fitted to sub-sequence (6 months)	0.358 ± 0.028	1.948 ± 0.218	3.635 ± 0.513

space–time distance of $r\tau$, in which r is the spatial distance between the events and τ is the time interval separating them. This type of analysis is based on the work by Zaliapin *et al.* (2008). The distribution of points in such a plot has also been shown to be bimodal, due to the same duality of types of neighbor events: siblings within a common sequence, which are clustered at short scales in time and distance, and unrelated events, which are more spatially and temporally distributed (Touati *et al.*, 2011). A straight line in Figure 2d indicates an approximate visual divide between the two distributions. This line has been reproduced in Figure 2e for comparison, which reveals that for the 15-month sequence period, the vast majority of points fall in the cluster relating to the aftershocks. (The position or even presence of the line is not crucial to make this observation; it merely facilitates comparison between the two plots.) Thus, these simple plots also support the possibility of viewing the sequence as consisting mostly of aftershocks.

Maximum-Likelihood ETAS Inversion

We start by fitting the ETAS model to three selections of data: the whole Colfiorito dataset, the 15-month sequence period selected by Lombardi *et al.* (2010) (from 3 May 1997 to 17 August 1998), and a shorter six-month subset of the sequence period containing the main peak in event rate (from 17 September 1997 to 17 March 1998), which we refer to as the subsequence. We use the Newton-based gradient descent algorithm *nlm* in R to minimize the negative of the log likelihood (LL), which for a point process is given by

$$\mathrm{LL} = \sum_i \log \lambda(t_i|H_{t_i}) - \int_{T_1}^{T_2} \lambda(t|H_t)dt, \qquad (3)$$

in which T_1 and T_2 delimit the temporal range of the events.

The results of this inversion are presented in Table 2, along with the branching ratio n, which is the average number of aftershocks produced per event, calculated as

$$n = \frac{Ac}{p-1}\frac{\beta}{\beta-\alpha}, \qquad (4)$$

in which $\beta = b \ln 10$. Lombardi *et al.* (2010) found that ML values for the stationary ETAS model did not sufficiently explain the sequence. For comparison, they obtained $n = 0.68$ and $\mu = 0.055$ for the whole dataset and $n = 0.79$ and $\mu = 0.13$ for the 15-month sequence period when fitting the stationary ETAS model to the Colfiorito dataset. Our results are thus somewhat similar, although not identical. Their paper states that they gathered 1586 events from the CSI; we only found 1527 events using the same selection criteria as stated in their paper, so perhaps this discrepancy, along with possible differences in the inversion algorithm, explains the difference in the result. However, it appears to be nonsignificant, as our result similarly underpredicts the event rate during the Colfiorito sequence, as we show next.

We check the fit using simulation modeling. We use our parameters for the whole dataset and the b-value calculated for the whole dataset ($b = 1.02$) to simulate the Colfiorito dataset repeatedly. To enable comparison with the real data, we add in the eight $M \geq 5$ events as part of the background process, because they affect the observed seismicity so greatly and we could not possibly obtain this exact pattern from random simulation. We suppress creation of other $M \geq 5$ events in the simulation to compensate for this addition. (We defer the question of how compatible this pattern of large events is with our model until the later section, Cluster of Large Events.) We can measure the average event rate in each of the three time periods considered in this study (over 100 realizations) and also calculate a standard deviation as a starting point to see how well we have matched the data. The results are shown in Table 3. We observe a systematic increase in average simulated event rate as we increasingly isolate the sequence in time, due to the larger number of aftershocks triggered by the $M \geq 5$ events. Additionally, the rates seem generally to be larger when the inversion of parameters has been carried

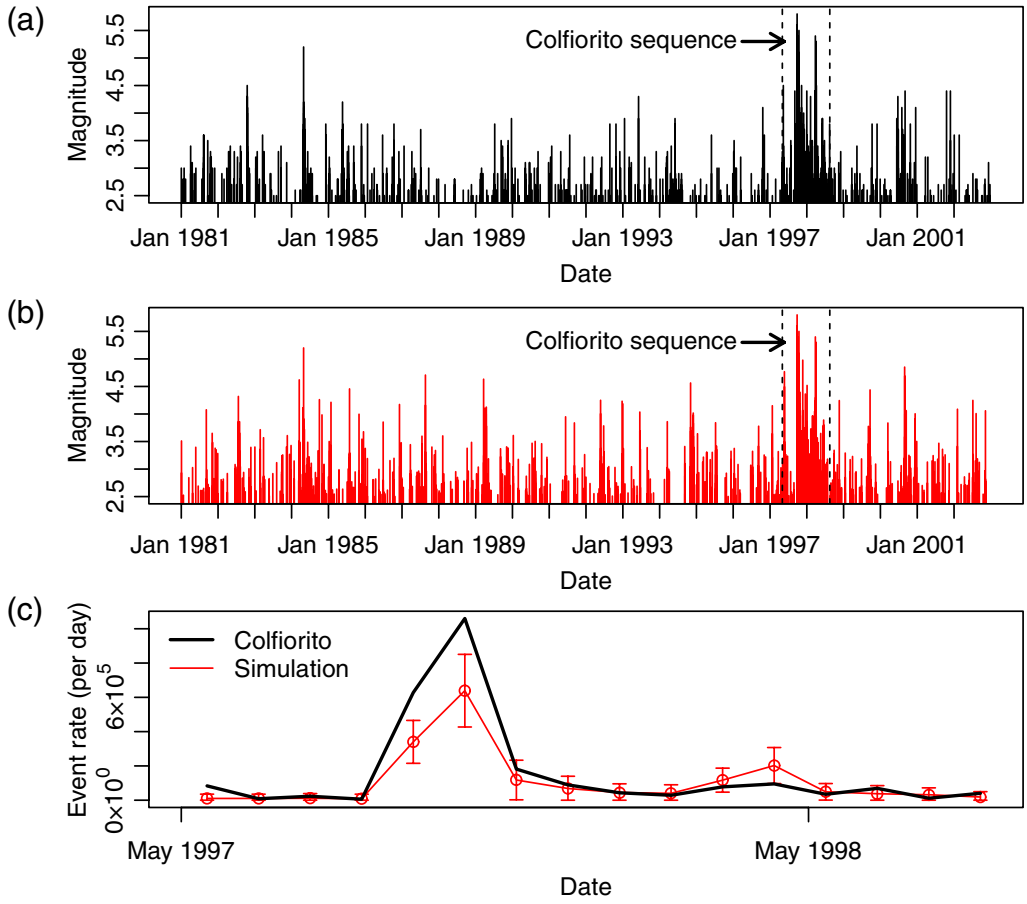

Figure 3. Comparison of Colfiorito data with simulations, using the temporal ETAS ML solution for the whole dataset, and with the $M \geq 5$ events included in the simulation as part of the background. Parts (a) and (b) show the magnitude time series for the Colfiorito data and for one realization of ETAS, respectively, whereas (c) compares the month-by-month event rates for a 15-month period that includes the sequence. The synthetic rate (thinner line with open circles) is an average across 100 simulations, with error bars representing two standard deviations (95% confidence limits). The color version of this figure is available only in the electronic edition.

out on the sequence period. However, none of the parameterizations provides a good match to both the overall (22-year) event rate and the rate during the sequence.

As an illustrative example, Figure 3a and 3b shows how one realization of the ML solution for the whole dataset (with the $M \geq 5$ events fixed as in the real data) compares with the real data, whereas Figure 3c shows details of the mean month-by-month event rates for both during the 15-month sequence period. A mean and standard deviation across all 100 realizations allows error bars representing 95% confidence limits to be plotted, which demonstrates that the real data falls outside of those limits around the time of peak rate. Thus, despite minor differences in the best-fit inverted parameters, we concur with Lombardi *et al.* (2010) that it seems difficult to fit the ETAS model to this sequence, regardless of whether we invert parameters for the whole dataset or for the sequence in isolation. However, before concluding that we must consider a time-varying background rate, we will consider the fact that there is an uncertainty associated with ML inversion and explore the possibility of finding a better, near-maximum-likelihood solution for the stationary ETAS model.

Improving the Fit by Exploring the Uncertainty

Motivated by the observation that small changes in the ETAS parameter values—well within the uncertainty of the inversion—can have comparatively large effects on the overall seismicity generated by the model, we explore the parameter space around the ML solution, using forward-modeling to assess the fit. It may be that, within the parameter uncertainty, there exists a stationary solution that describes the data adequately well, including both the sequence and the overall event rate. We use the whole-dataset case in this analysis because it is based on the largest amount of data, and we wish to model the whole dataset.

We assume the likelihood surface close to the solution may be approximated by a Gaussian distribution. Our procedure for this exploration is therefore to sample all parameter values from a multivariate Gaussian distribution with mean equal to the ML solution and standard deviation equal to the covariance matrix, obtained by solving the Hessian matrix output from the inversion. This gives a candidate alternative solution, which we reject immediately if any of the parameters have negative values or the branching ratio does

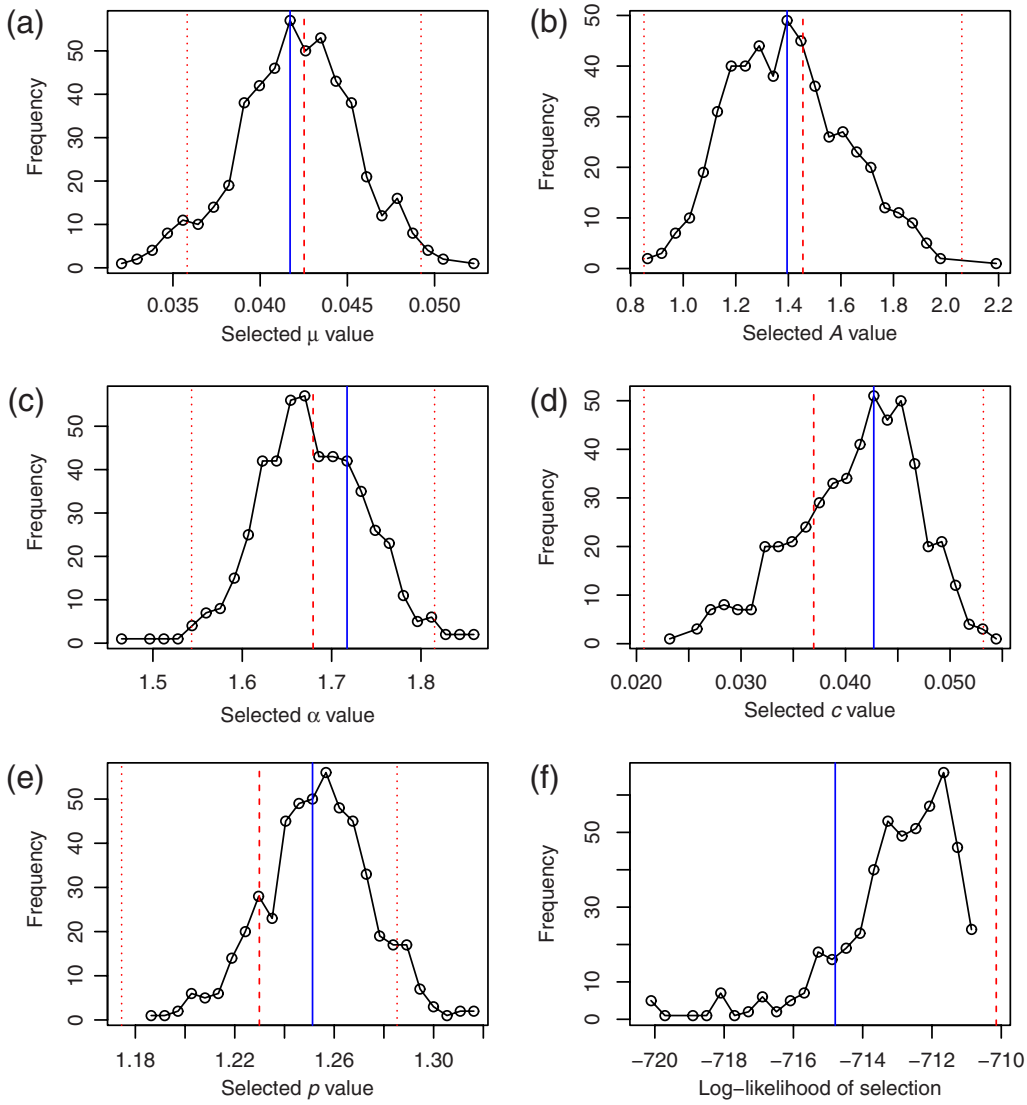

Figure 4. (a)–(e) Histograms of parameter values accepted from Gaussian sampling around the ML temporal solution, using the covariance matrix from the inversion; acceptance is based on an adequate fit in forward modeling, as described in the text. In each plot, the dotted vertical lines indicate the standard error, with the ML value as a dashed line in the center; the solid vertical line shows the selected alternative solution. (f) Histogram of log-likelihood values for the accepted sets of parameter values, with the maximum log likelihood shown as a vertical dashed line and the log likelihood for the selected alternative parameters shown as a solid line. The color version of this figure is available only in the electronic edition.

not lie in the range $0 \leq n < 1$. We then analytically test the total event rate r using the formula $r = \frac{\mu}{1-n}$ (Helmstetter and Sornette, 2003a). If this is greater or smaller than the Colfiorito dataset's mean event rate by a factor of more than 0.1, we reject it also. (This is just a guide, as it is a theoretical mean, taking into account extreme events; in practice, the observed event rate is likely to be lower, assuming a finite time period.) Assuming it passes these tests, we then simulate the Colfiorito dataset using these parameters. The final check is then to compare the simulated event rate with the real rate during the periods of elevated rate around the big events. We look at two specific time periods corresponding to the two clusters of $M \geq 5$ events (and the elevated-rate periods that follow them): 26 September 1997–25 March 1998 and 26 March–22 September 1998. We now reject the parameterization if the rate during either of these periods is greater or smaller than that of the real data by a factor of more than 0.2. If the parameterization is ultimately accepted, we record the parameter values and their log likelihood. This is then repeated until we have accepted 500 sets of parameter values.

Figure 4a–e shows histograms of the parameter values accepted using this procedure, whereas Figure 4f shows a histogram of the log likelihood of those parameterizations. Some of the parameter histograms are significantly nonsymmetrical and do not peak on the ML solution. This shows that our selection criteria relating to event rates have effectively altered the likelihood surface slightly. The log likelihood is more commonly close to the maximum than further away;

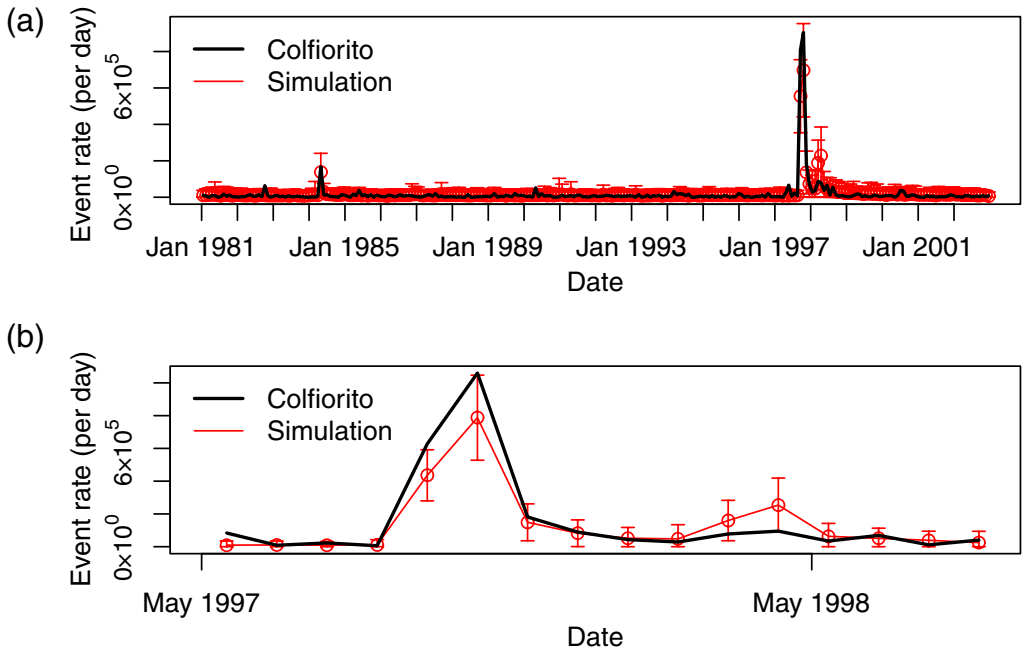

Figure 5. Month-by-month event rates for simulations using the alternative parameter values shown in Figure 4, compared with the real event rate, for (a) the whole dataset and (b) a 15-month period including the sequence. The synthetic rate (thinner line with open circles) is, again, an average across 100 simulations, with error bars representing two standard deviations (95% confidence limits). The color version of this figure is available only in the electronic edition.

this reassures us that we are tending to find high-likelihood alternatives.

We choose a single alternative solution by looking at the parameter values with the highest counts. Rather than simply choose the peak values, we try a few combinations from the highest-count values and make the final selection based on a balance between the visual match to the data in forward modeling (performing the same simulation analysis as we showed in Fig. 3 for the ML solution) and the value of the log likelihood. This is a somewhat subjective step, but, having shown in Figure 4a–4e that alternative sets of parameter values (close enough to the ML solution to be within the allowable error range) can easily be found that appear to better explain the data, we now simply wish to select a representative single set for further forward-modeling analysis.

Solid vertical lines in Figure 4a–e show the values we selected as our alternative parameterization. These values are $\mu = 0.042$, $A = 1.395$, $\alpha = 1.717$, $c = 0.043$, and $p = 1.251$, giving a branching ratio of $n = 0.886$. Similarly, in Figure 4f, a solid vertical line indicates the log likelihood of this selection. The likelihood value is high enough to be able to say that this is not an extreme selection, even within the limited space that is sampled around the peak likelihood.

Figure 5 shows the month-by-month event rate for 100 ETAS simulations performed with these alternative values. Visually, they provide a significantly better match to the data than the ML solution; indeed, the real event rate comes within the 95% confidence intervals of the simulations at the peak, even in Figure 5b, which shows the evolution of the event rate over much narrower time windows around the biggest peak. The fit to the long-term rate outside of the sequence is also excellent.

Figure 6 replots the interevent time histograms of Figure 2b and 2c, along with their synthetic counterparts from simulation of the ETAS ML solution and the alternative parameters obtained through the sampling procedure. Both of these options produce histograms that agree very well with the Colfiorito data; agreement is slightly greater for the alternative parameters in Figure 6b, in which the counts during the highest-rate (shortest interevent times) portion of the sequence are systematically lower using the ML parameters.

We can also look at the relative proportions of correlated interevent times (arising from aftershocks in the same sequence) and uncorrelated intervals (arising from unrelated event pairs) for the simulations. Figure 7 shows these two components superposed for one realization of ETAS using the alternative solution. The two components each have a peak in the histogram in the expected places for the whole dataset. Also, we can see that the 15-month sequence period in Figure 7b is dominated by correlated aftershock pairs (the correlated peak is nearly an order of magnitude higher than the uncorrelated peak). This further supports our hypothesis that aftershocks are mostly responsible for the raised event rate in this period. If the background rates instead were elevated over the sequence period, we would expect to see a more exponential distribution (Touati *et al.*, 2009). This is because, even though the time series itself would be dominated by the aftershocks of these background events, the aftershocks would take the form of numerous distinct sequences overlapped in time. Thus, successive events in the catalog would most often be independent from

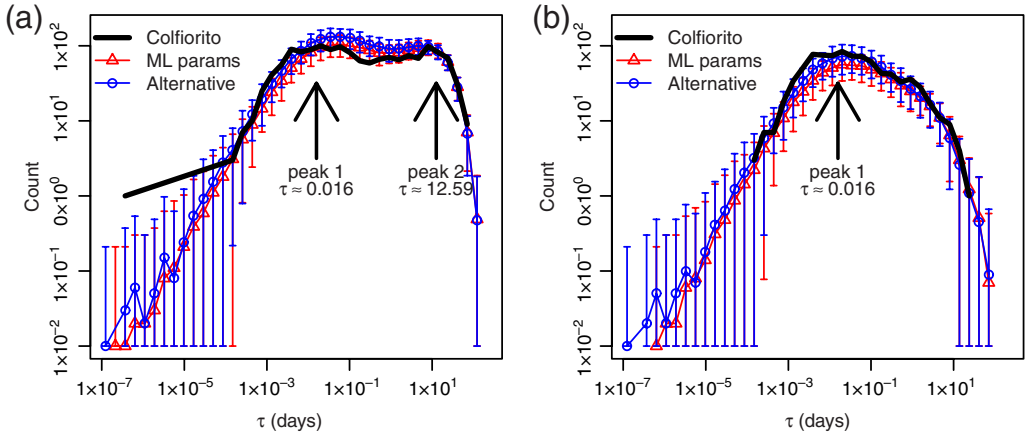

Figure 6. Interevent time histograms for (a) the whole Colfiorito time period and (b) the sequence period only (3 May 1997–17 August 1998), comparing the real data with simulations from the temporal ETAS ML solution and the alternative proposition from the Gaussian sampling exercise of Figure 4. The points with error bars represent mean ±2 standard deviations over 100 realizations. Both ETAS models match the data well; the alternative is slightly better, especially during the sequence. The color version of this figure is available only in the electronic edition.

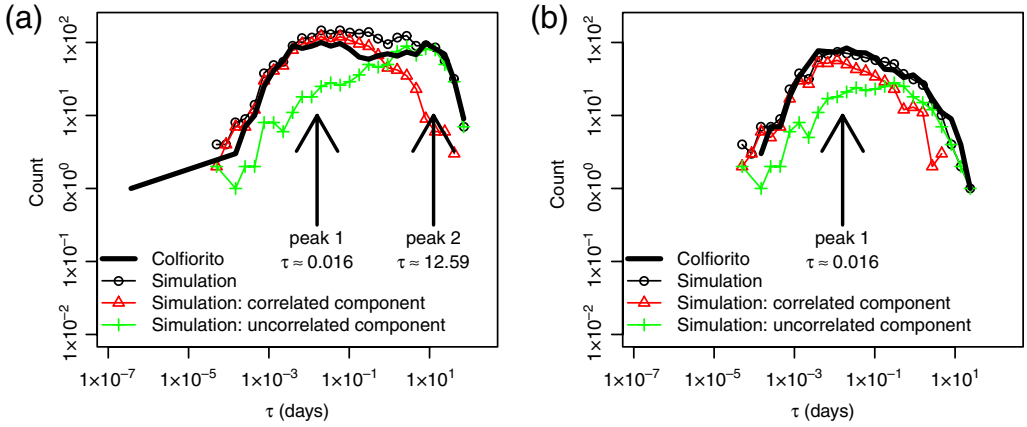

Figure 7. Similar to Figure 6, but with only one realization of the ETAS model plotted (alternative parameters) and showing a breakdown of the interevent times that are correlated (triangles) and uncorrelated (crosses), which may be determined only for the simulation (and not for the real data). "Correlated" means that the interval occurs between two events that are part of a common aftershock sequence, whereas "uncorrelated" means the events are unrelated. Note that the 15-month sequence period (b) appears to consist mostly of aftershocks, at least in the simulation. The color version of this figure is available only in the electronic edition.

each other, and so the distribution of intervals between successive events would be dominated by the exponential, independent component. What we are seeing here is more consistent with few aftershock sequences that, although they contain many events, are sufficiently isolated in time that the power-law signature of their occurrence intervals shows in the histogram.

To test whether the interevent time distribution can distinguish between our stationary ETAS model and a model with a varying background rate such as that used by Lombardi *et al.* (2010), we simulate the latter, and plot the histograms. We do not know the specific values of μ obtained in the moving-window analysis of Lombardi *et al.* (2010), but we can approximate it by looking at their figure 5a. We use our ML value, $\mu = 0.043$, until 1 October 1997, at which point we increase it to $\mu = 1.75$. We then decrease to $\mu = 1$ on 1 November 1997, decrease again to $\mu = 0.75$ on 1 December 1997, and finally revert to the ML value on 1 September 1998. The other parameters are kept at their ML values throughout, and the nine large $M \geq 5$ events are added to the background, as with the stationary model.

A plot equivalent to Figure 3 for this simulation (not shown) reveals that the overall event rate indeed is more comparable to the real data than the stationary ML model, although our alternative model still performs better by this measure. The interevent time histogram for the varying-background simulation is shown in Figure 8. The resemblance to the Colfiorito data is not as good as for the stationary model; in particular, during the sequence period (Fig. 8b), the varying-background histogram is more broadly rounded and less gamma-like in shape. This is the result of effectively mixing several distributions by varying μ.

A nearest-neighbor analysis is shown in Figure 9, analogous to that shown in Figure 2d and 2e, with the Colfiorito data in the top left and bottom left plots and stationary ETAS

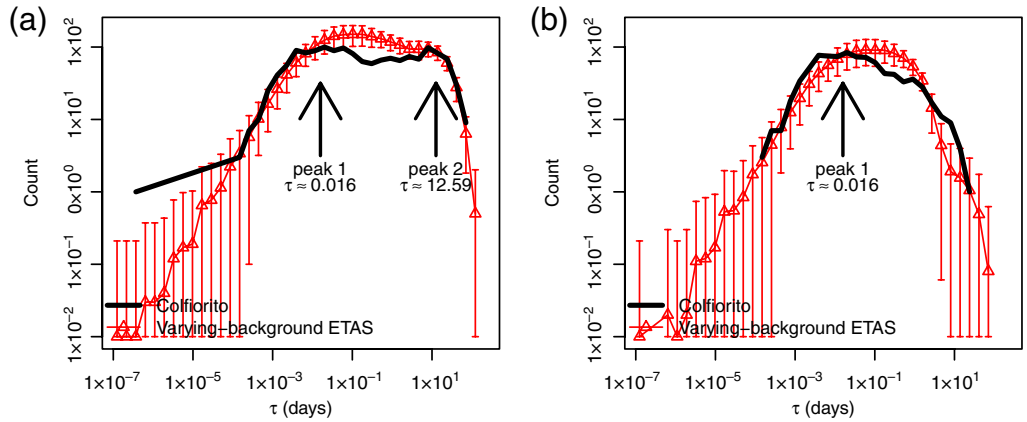

Figure 8. Interevent time histograms for (a) the whole Colfiorito time period and (b) the sequence period only (3 May 1997–17 August 1998), comparing the real data with simulations from the temporal ETAS with varying background rate as described in the text. The points with error bars represent mean ±2 standard deviations over 100 realizations. The resemblance to the real data is worse than the models shown in Figure 6. The color version of this figure is available only in the electronic edition.

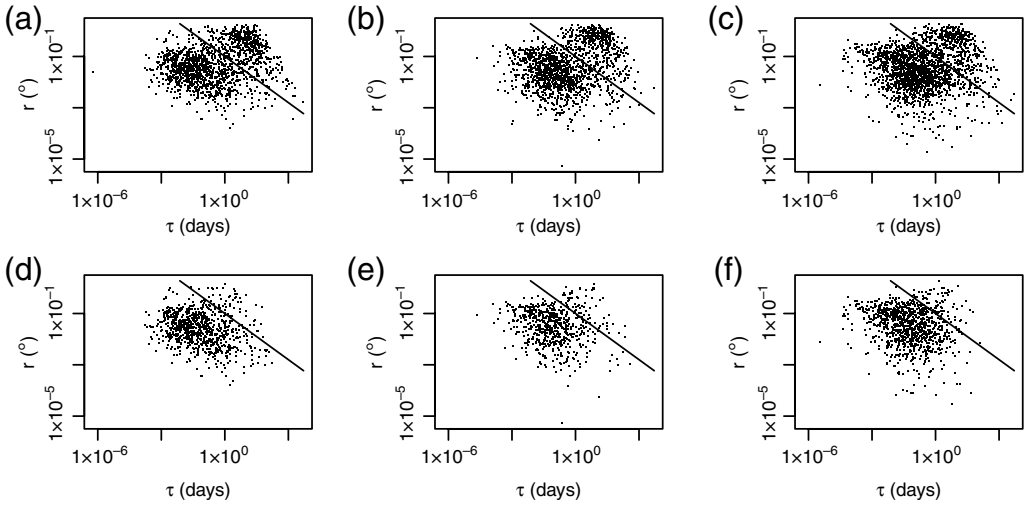

Figure 9. Space–time nearest-neighbor plot for the whole time period (upper row) and the 15-month sequence period only (lower row), (a, d) comparing the real data with (b, e) one simulation each from the ETAS ML solution and (c, f) the alternative proposition (from the Gaussian sampling exercise of Fig. 4).

simulations in the other plots. The simulations here were performed using a spatiotemporal ETAS model (equation 2) with $d = 0.000062$, which was obtained by fitting the spatiotemporal model to the whole dataset while keeping the temporal parameters (μ, A, α, c, and p) fixed at the ML values obtained in Table 2. This value of d nominally characterizes the spatial distribution of aftershocks around parent events, allowing a simple way to simulate a catalog of spatial as well as temporal data; we do not attempt to spatially model the background process in a realistic way but merely simulate this uniformly in space.

For the ETAS simulations, we superpose the straight dividing line from the nearest-neighbor plot of the real data (Fig. 9a,d, also shown and explained in Fig. 2d,e), and find that it separates the synthetic clusters very well also. Overall, there is visual similarity between the real and synthetic data in these plots, even though the spatial aspect of the modeling is overly simplistic; the simulations have produced some short distances that are below the spatial resolution limits of the real data, but the clusters occur in the same regions of the plot with similar relative populations of points. This adds to the support for our alternative parameters.

For comparison with Lombardi *et al.* (2010), we show two types of residual analysis for our ML and alternative ETAS models: the residual point process (RPP) and an inferred cumulative background (Fig. 10). The RPP in Figure 10a consists of transformed event times, obtained by integrating the conditional intensity (equation 1) from the start up to each event time in the real data, using the specified model parameters. This should transform the event times to approximately a Poisson process of unit rate if the model is a good fit to the data (Ogata, 1988). The inferred background

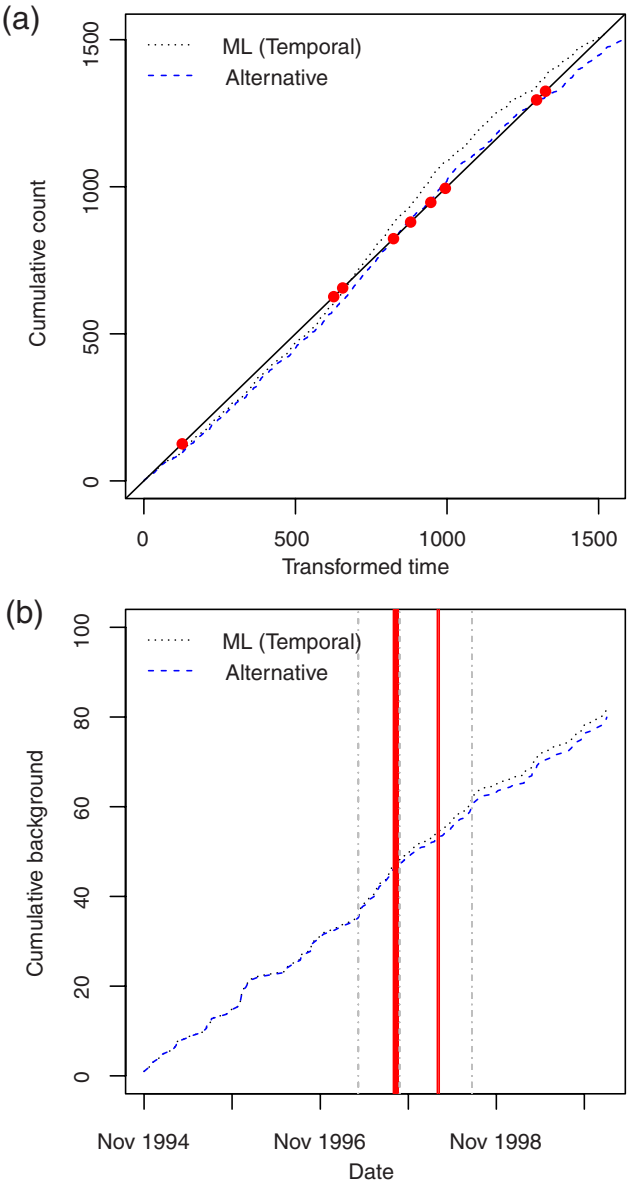

Figure 10. (a) Residual point process analysis on the Colfiorito data using the two different parameterizations of ETAS. The transformed time on the x axis is the integral of the conditional intensity from the start up to each event time; the solid straight line represents the expected count as a function of transformed time if the model is a good fit. The large $M \geq 5$ event occurrence times are shown as dots along this line. (b) The inferred cumulative background events are shown as a function of time for September 1994–March 2000, as in Lombardi *et al.* (2010), using each of the three parameterizations to infer this. Vertical dashed-dotted lines indicate the change points found by Lombardi *et al.*, and vertical solid lines show the times of the $M \geq 5$ events. The color version of this figure is available only in the electronic edition.

in Figure 10b is obtained by thinning the catalog based on the stochastic identification of aftershocks (Schoenberg, 2003; Zhuang *et al.*, 2005). The thinned process is then taken to represent the background and can be plotted as a cumulative function of time to check for stationarity. This technique comes from the stochastic declustering of Zhuang *et al.* (2002), in which, after ETAS parameters for the catalog have been determined, each event may be assigned a probability of being triggered by any of the previous events and (conversely) a probability p_{bg} of being background:

$$p_{\mathrm{bg}} = \frac{\mu}{\lambda(t|H_t)} = \frac{\mu}{\mu + \mathrm{AS}}, \tag{5}$$

in which AS refers to the aftershocks term of ETAS, evaluated with the current event history. Deviations from linearity in the cumulative background probability as a function of time may be taken to indicate that the stationary ETAS model in question does not match the data well.

In Figure 10a, the residual point process of the alternative parameterization is noticeably more stationary than that of the ML solution and, after the second and third large event, stays closer to the ideal (indicated by a straight line). Figure 10b shows the inferred background over the same range of dates used in figure 4b of Lombardi *et al.* (2010), and vertical dashed lines indicate the change points identified visually by Lombardi *et al.* It is interesting to note that the two curves lie on top of each other initially, start to diverge at the first change point, and become even more so at the second. The apparent change points are markedly less noticeable with the alternative parameters in terms of an event rate increase. The inferred background rate does still appear to increase at the first change point, but we note that there is a similar or even greater visible fluctuation around the beginning of 1996, which does not correspond to a marked increase in the event rate in Figure 2a. Thus, whether real or not, these apparent changes in background do not appear to be tightly correlated with the type of activity seen in the Colfiorito sequence.

Cluster of Large Events

We now turn our attention to the question of the likelihood of seeing clusters of large $M \geq 5$ events in ETAS similar to the ones in the Colfiorito data, which we have so far simply transplanted into our simulation modeling. One obvious place to start is to check whether these events violate the Gutenberg–Richter law. The b-value for the 15-month sequence period is 0.955, slightly smaller than that for the whole dataset ($b = 1.02$), which reflects a greater proportion of larger events during this time; it is not abnormally low, however. We can plot a histogram and compute 95% confidence intervals from a Poisson distribution around the ML frequency at each magnitude bin. We can also place counting error bars on the measured frequencies: the 95% confidence limits of a binomial error distribution happen to be equal to the inverse of the cumulative beta distribution, evaluated at 0.975 and 0.025, multiplied by the total count. Figure 11 shows examples of this for the 15-month sequence period. None of the data sections or sections of simulations exhibit a significant deviation from Gutenberg–Richter in terms of measured frequencies falling outside of the confidence intervals at large magnitudes.

Next, we can look at the average spontaneous occurrence rates of these clusters in ETAS simulations, using both the ML parameters for the whole dataset and the alternative parame-

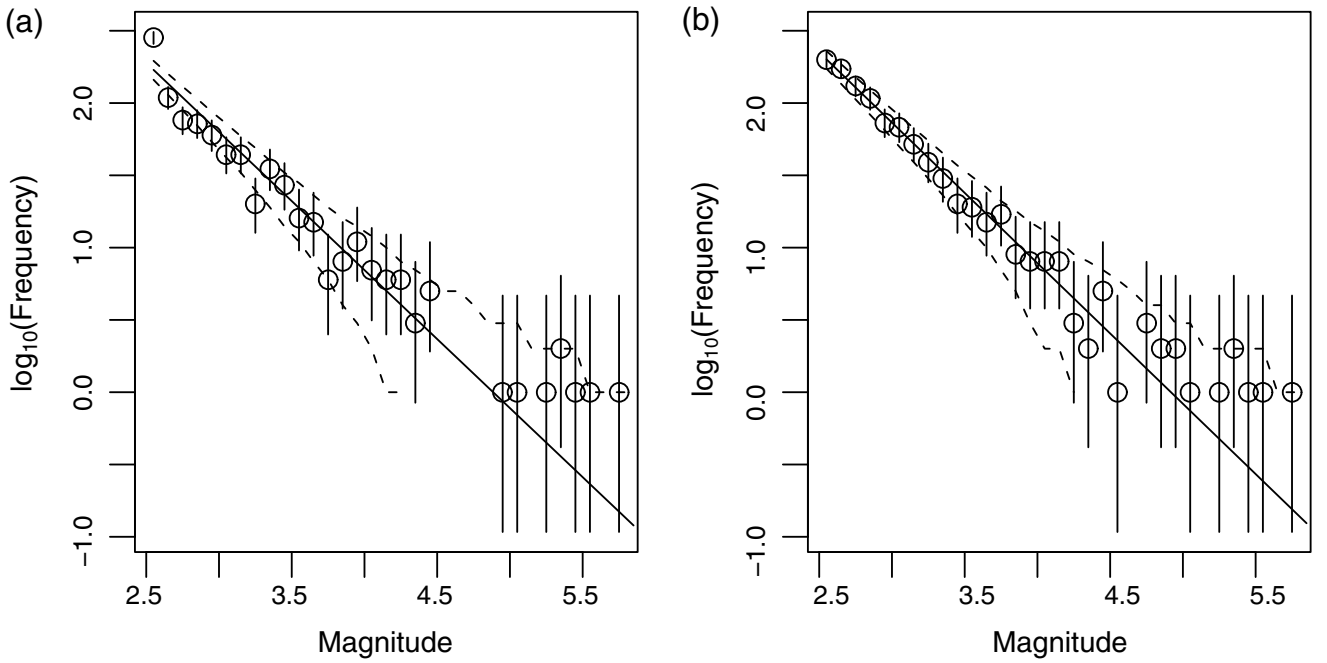

Figure 11. Frequency–magnitude plot for the sequence period 3 May 1997–17 August 1998, with Gutenberg–Richter fit (straight line) and 95% confidence limits (dashed lines): (a) the real data; (b) the ETAS simulation with the alternative parameters. The points, with their counting errors as indicated, are consistent with the Gutenberg–Richter law in both cases.

ters. Although magnitudes in ETAS simulations are each selected independently from the Gutenberg–Richter distribution, there are small but significant temporal correlations between the magnitudes. This is due to the fact that, when the event rate during a time period δt is elevated (as is the case following a large event), the probability of seeing a large event within δt is also elevated (Helmstetter and Sornette, 2003b). Thus a cluster of large events in an ETAS simulation is more likely than in a stationary Poisson process without aftershocks (and its likelihood also varies with the parameter values). Looking for such a cluster emerging in an ETAS simulation also does not force the large events to be independent, as they were in our forward-modeling, but allows the possibility of them arising as part of a triggered sequence.

We run simulations for 22 years each (the duration of the CSI), producing 100,000 realizations of each model, and then look for the occurrence of clusters of six $M \geq 5$ events within 19 days, as seen in the Colfiorito data between 29 September and 14 October 1997. We observe at least one such cluster in 4.54% of the 22-year simulations for the alternative parameters and in 2.29% of simulations with ML parameters. We notice that the frequency increases with the number of realizations. Convergence of rates of extreme events, such as this cluster, toward their true long-term mean value, is very slow and occurs in an upward direction (Naylor *et al.*, 2008); these estimates are therefore lower limits. The mean number of occurrences of such a pattern is 0.064 times per 22-year simulation in the alternative model, compared with 0.027 times for the ML parameters. The standard deviations are 0.493 and 0.225, respectively; these are an order of magnitude greater than the mean, showing how uncertain the estimates of mean rates for such extreme events can be. We note also that in defining the cluster, we have selected a time window (19 days) that maximizes the apparent anomaly: we could have used a wider window and included more than six events, but this would have given us a lower event rate of $M \geq 5$ events. Alternatively, we could have used a smaller window and made the cluster smaller in size, and thus easier to match. Of all the possible ways of expressing our cluster, we have used the form that gives us the most anomalous-looking set of events. Shearer and Stark (2012) point out that such selection procedures are subjective and warn against defining apparent anomalies too specifically, because any highly specific pattern, interesting or otherwise, will inherently be a highly unlikely event.

A cluster of six $M \geq 5$ events in 19 days occurred roughly twice as frequently in our simulations of the alternative parameterization than in the ML solution. This must be due to the very small difference in branching ratio between these two (0.886 compared with 0.824); their background or independent event rates are almost equal. The approximate doubling of the cluster occurrence rate with the alternative parameters again shows how uncertain this rate is and how sensitive it is to such a difference in an important parameter (which in itself is rather uncertain). The origin of the cluster here remains a question open for further investigation, especially given that there is a proposed physical mechanism of fluid-driven triggering; however, in our analysis we cannot reject that it may be a chance outcome of the normal stationary seismicity of the region. We also note that even with a varying background rate as utilized by Lombardi *et al.* (2010), the

large events still need to be included in order to see comparable event rates during the sequence from a simulation. Thus, the question of the origin of this cluster of large events remains, regardless of whether a stationary or nonstationary ETAS model is used to represent the Colfiorito dataset.

Discussion

We have shown in our Gaussian sampling of ETAS parameters (Improving the Fit by Exploring the Uncertainty section) that if we specify that the average event rate for the model must match that of the data (within some particular range), we may obtain an alternative solution that visually matches the data better than the ML fit. This at first glance seems controversial; ML, after all, obtains the set of parameter values that give the highest likelihood of observing the data. Why, then, do the simulations of the ML fit look so different from the data?

To say that a set of parameters give the highest likelihood of observing a specific set of data does not imply that the data represent the most likely outcome of that parameterization. This may not be the case. Thus when we simulate the model, the synthetic data, which will be closer to the most likely outcome of the model, may be quite different in terms of readily observable attributes, such as the event rate. As an obvious example, it is possible to fit ETAS with ML and obtain a branching ratio (equation 4) of greater than 1, which leads to the unphysical situation of an unbounded event rate when simulated.

Reasons for this mismatch can include the fact that the data are a finite sample of the underlying process, covariances in the model parameters, relative flatness of the likelihood surface, and limitations of the model in representing real data.

ML parameter inversion for the ETAS model is not constrained by the overall event rate or total number of events. The likelihood is formed by simply taking the probability density for the occurrence time of the next event (given the history at that time, and specified by the model), evaluating it at the time at which the next event actually occurred, and multiplying this together for all events in the dataset. Thus it tries to match patterns of event occurrence in time, rather than overall event rates.

Under some conditions, it consistently arrives at the wrong answer. For example, we previously showed (using simulations) that in datasets that span a very large geographical area, the high degree of temporal overlapping of aftershock sequences can mask the triggering pattern, leading to systematic overestimation of the background rate and underestimation of the branching ratio by the ML technique (Touati *et al.*, 2011). In that case, essentially there are many possibilities to match the seismicity pattern, which resembles a Poisson process in time. In light of our present study, we would interpret such a result in terms of a large parameter uncertainty, as well as a bias in the position of the peak likelihood. In our simulation with $\mu = 10$ events per day (Touati *et al.*, 2011), the true solution was not even within the 95% confidence interval of the inversion; thus, exploring within the confidence interval as we have done in this paper may even be considered conservative, as it can be an underestimation of the true error.

In the case of the Colfiorito data, we have found that observable attributes such as the event rate can vary considerably within the vicinity of the ML solution. In the case of strongly overlapping aftershock sequences, perhaps exploring the uncertainty would similarly give rise to significant changes in the branching ratio and background rate, even if the overall event rate was more stable in that case. The sensitivity of the average simulation outcome to changes in the parameters is demonstrably much greater than the sensitivity of the likelihood to changes in those parameters, for a particular set of data. This is the key observation underpinning our sampling around the peak likelihood.

The results of this paper suggest that it may be useful to think of ML as being not simply the peak in likelihood, but a subset of model space around the peak, defined by the confidence interval. The event rate can also be a useful further constraint for selecting model parameters from within that space. The results also demonstrate that the inversion uncertainty should be taken into account and explored before assigning significance to apparent rate changes.

Conclusions

We have analyzed the Colfiorito earthquakes over 22 years and attempted to model the seismicity using ETAS by ML fitting combined with forward modeling and comparison on various metrics. Despite slight differences in procedure, we agree with Lombardi *et al.* (2010) that the ML parameters for the whole dataset tend to lead to insufficient earthquake productivity during the sequence of 1997–1998. We have explored the parameter space around the ML solution, within the uncertainty inherent in the inversion procedure, and found that we can significantly change the result using just a small change in the parameter values. With the nine $M \geq 5$ events transferred from the Colfiorito dataset into the simulation background, we see event rates that compare (within error) with the real seismicity throughout the catalog, better than for a model with a varying background as used by Lombardi *et al.* (2010). We also find a convincing visual match to the data when looking at interevent time histograms and space–time nearest-neighbor plots. These plots reveal the triggering structure of the simulated data for $M < 5$, and the similarities with the real data strongly indicate that the sequence consists largely of aftershocks generated by some few large events. In particular, the histogram of interevent times during the sequence period resembles that of a gamma distribution, which is more consistent with aftershocks occurring successively (Touati *et al.*, 2009) than with a varying background rate (as shown in Fig. 8b).

By sampling the parameter space, we have essentially imposed an additional constraint on the parameter selection: that the average event rate of the model must match that of the data, a constraint that is absent from the ML inversion. This has allowed us to find a parameterization of the ETAS

model that matches the aftershock production during the sequence within the 95% confidence intervals, reducing or removing the need to increase the background rate during this period while still matching the data in the long term. This suggests that the seismicity over the 22 years can be considered to be generally stationary.

We have also looked at the likelihood of obtaining the clusters of large events from our ETAS models. It is not trivial to set an expectation on how infrequently a particular pattern should arise by chance for it to be deemed anomalous when it does appear within a 22-year catalog. Any highly specific pattern is, inherently, highly unlikely. However, we found that a cluster of six $M \geq 5$ events in 19 days occurred more frequently by chance in our simulations of the alternative parameterization than in the ML solution. It occurred in 4.54% of our 22-year simulations; due to slow upward convergence, this can be deemed a lower limit on the true frequency. We do not think this is rare enough to reject that the cluster of events triggering the Colfiorito sequence may be part of the normal long-term seismicity of the region as captured by ETAS.

Data and Resources

We used data from the Catalogo della Sismicità Italiana —CSI 1.1, downloaded from http://csi.rm.ingv.it/versione_inglese/index_eng.htm (last accessed 4 October 2013).

We made use of some of the R functions in Statistical Seismology Library (SSLib), available at http://homepages.maxnet.co.nz/davidharte/SSLib/ (last accessed 4 October 2013).

Acknowledgments

This research was carried out in the framework of the REAKT Project (Strategies and Tools for Real-Time EArthquake RisK ReducTion) founded by the European Community via the Seventh Framework Program for Research (FP7), Contract Number 282862. S. T. was funded by REAKT. M. N. was funded by a Scottish Government and Royal Society of Edinburgh Research Fellowship. The manuscript was greatly improved by feedback from two anonymous referees. We are also grateful for initial data from and helpful discussions with Anna Maria Lombardi, Warner Marzocchi, and Massimo Cocco.

References

Castello, B., M. Olivieri, and G. Selvaggi (2007). Local and duration magnitude determination for the Italian Earthquake Catalog, 1981–2002, *Bull. Seismol. Soc. Am.* **97,** 128–139.

Castello, B., G. Selvaggi, C. Chiarabba, and A. Amato (2005). *CSI Catalogo della sismicità italiana 1981–2002, vers. 1.0*, Istituto Nazionale di Geofisica e Vulcanologia-Centro Nazionale Terremoti, Rome, http://csi.rm.ingv.it/versione_inglese/index_eng.htm (last accessed November 2012) (in English).

Harte, D. (2012). Statistical Seismology Library (SSLib) package 'ptprocess,' version 3.3–1, http://homepages.maxnet.co.nz/davidharte/SSLib/ (last accessed February 2014).

Helmstetter, A., and D. Sornette (2003a). Importance of direct and indirect triggered seismicity in the ETAS model of seismicity, *Geophys. Res. Lett.* **30,** no. 11, 1576.

Helmstetter, A., and D. Sornette (2003b). Bath's law derived from the Gutenberg–Richter law and from aftershock properties, *Geophys. Res. Lett.* **30,** no. 20, 2069.

Lindman, M., K. Jonsdottir, R. Roberts, B. Lund, and R. Bodvarsson (2005). Earthquakes descaled: On waiting time distributions and scaling laws, *Phys. Rev. Lett.* **94,** no. 10, 108501.

Lombardi, A. M., M. Cocco, and W. Marzocchi (2010). On the increase of background seismicity rate during the 1997–1998 Umbria–Marche, Central Italy, sequence: Apparent variation or fluid-driven triggering? *Bull. Seismol. Soc. Am.* **100,** no. 3, 1138–1152.

Miller, S. A., C. Collettini, L. Chiaraluce, M. Cocco, M. Barchi, and B. J. Kaus (2004). Aftershocks driven by a high-pressure CO_2 source at depth, *Nature* **427,** no. 6976, 724–727.

Molchan, G. (2005). Interevent time distribution in seismicity: A theoretical approach, *Pure Appl. Geophys.* **162,** no. 6–7, 1135–1150.

Naylor, M., I. G. Main, and S. Touati (2008). Quantifying uncertainty in mean earthquake interevent times for a finite sample, *J. Geophys. Res.* **114,** no. B01316, doi: 10.1029/2008JB005870.

Ogata, Y. (1988). Statistical models for earthquake occurrences and residual analysis for point processes, *J. Am. Stat. Assoc.* **83,** no. 401, 9–27.

Ogata, Y. (1998). Space-time point-process models for earthquake occurrences, *Ann. Inst. Stat. Math.* **50,** no. 2, 379–402.

Romashkova, L., and A. Peresan (2013). Analysis of Italian earthquake catalogs in the context of intermediate-term prediction problem, *Acta Geophys.* **61,** no. 3, 583–610.

Saichev, A., and D. Sornette (2006). "Universal" distribution of interearthquake times explained, *Phys. Rev. Lett.* **97,** no. 7, 078501.

Saichev, A., and D. Sornette (2007). Theory of earthquake recurrence times, *J. Geophys. Res.* **112,** no. B04313, doi: 10.1029/2006JB004536.

Schoenberg, F. P. (2003). Multidimensional residual analysis of point process models for earthquake occurrences, *J. Am. Stat. Assoc.* **98,** no. 464, 789–795.

Shearer, P. M., and P. B. Stark (2012). Global risk of big earthquakes has not recently increased, *Proc. Natl. Acad. Sci. Unit. States Am.* **109,** no. 3, 717–721.

Touati, S., M. Naylor, and I. G. Main (2009). Origin and nonuniversality of the earthquake interevent time distribution, *Phys. Rev. Lett.* **102,** no. 16. 168501.

Touati, S., M. Naylor, I. G. Main, and M. Christie (2011). Masking of earthquake triggering behavior by a high background rate and implications for epidemic-type aftershock sequence inversions, *J. Geophys. Res.* **116,** no. B03304, doi: 10.1029/2010JB007544.

Traversa, P., and J.-R. Grasso (2010). How is volcano seismicity different from tectonic seismicity? *Bull. Seismol. Soc. Am.* **100,** no. 4, 1755–1769.

Zaliapin, I., A. Gabrielov, V. Keilis-Borok, and H. Wong (2008). Clustering analysis of seismicity and aftershock identification, *Phys. Rev. Lett.* **101,** no. 1, 018501.

Zhuang, J., C. P. Chang, Y. Ogata, and Y. I. Chen (2005). A study on the background and clustering seismicity in the Taiwan region by using point process models, *J. Geophys. Res.* **110,** no. B05S18, doi: 10.1029/2004JB003157.

Zhuang, J., D. Harte, M. J. Werner, S. Hainzl, and S. Zhou (2012). Basic models of seismicity: Temporal models, *Community Online Resource for Statistical Seismicity Analysis*, doi: 10.5078/corssa-79905851, available at http://www.corssa.org/articles/themev/zhuang_et_al_a (last accessed February 2014).

Zhuang, J., Y. Ogata, and D. Vere-Jones (2002). Stochastic declustering of space-time earthquake occurrences, *J. Am. Stat. Assoc.* **97,** no. 458, 369–380.

University of Edinburgh
School of GeoSciences
Grant Institute
West Mains Road
Edinburgh EH9 3JW, United Kingdom

Manuscript received 21 October 2013;
Published Online 18 March 2014